JGR Space Physics

RESEARCH ARTICLE
10.1029/2020JA028513

The Location of the Earth's Magnetic Poles From Circum-Terrestrial Observations

M. Regi[1], D. Di Mauro[2], and S. Lepidi[1]

[1]Istituto Nazionale di Geofisica e Vulcanologia, L'Aquila, Italy, [2]Istituto Nazionale di Geofisica e Vulcanologia, Rome, Italy

Key Points:

- The dip poles positions at Swarm satellite altitudes are identified by robust although simple method
- Westward and northward dip poles drift is rigorously found confirming an higher velocity for the north dip pole
- The identified dip poles positions from experimental observations and models are compared

Correspondence to:
M. Regi,
mauro.regi@ingv.it

Citation:
Regi, M., Di Mauro, D., & Lepidi, S. (2021). The location of the Earth's magnetic poles from circum-terrestrial observations. *Journal of Geophysical Research: Space Physics*, *126*, e2020JA028513. https://doi.org/10.1029/2020JA028513

Received 22 JUL 2020
Accepted 24 NOV 2020

Abstract The magnetic poles or dip poles are the points on the Earth's surface and circum-terrestrial area where the magnetic field is vertical, so the horizontal component vanishes. They are not coincident with geomagnetic poles, which are the points where the dipole axis, obtained by analytic models, intersects the Earth's surface, and their instrumental sampling determination from ad hoc ground surveys is difficult due to the harsh environmental conditions and remoteness of the areas where they are located. In this work, we use magnetic field measurements from ESA's Swarm satellites covering 5 years (2015–2019), and determine the position of the magnetic poles by modeling the yearly average horizontal magnetic field component through analytic two-dimensional Taylor polynomial fit and finding the locations where this component is minimum. The yearly dip poles positions at average satellites geocentric altitudes are also projected at ground level based on WGS84 geodetic reference system. Reliability of our method is evaluated by an optimized Monte Carlo test applied to combined International Geomagnetic Reference Field (IGRF) model and Swarm data. The availability of several years of data allows us to investigate the long term variation and dynamics of the magnetic poles, also in comparison with the results provided by IGRF model (both IGRF12 and IGRF13). Our results agree with the model, in better accordance in the north hemisphere with IGRF13, indicating that both magnetic poles move in the north-west direction, with a speed of ∼37–72 km/y (lower in year 2016) for the north dip pole and of ∼5–9 km/y for the south one.

1. Introduction

The regular observations of the Earth's magnetic field from different points of the planet, older than those of meteorology and seismology, allowed Gauss since mid of 19th century to reconstruct from the spherical harmonic analysis that the main contribution to the field comes from its internal dipolar component. The quality of the Gauss analytic models has been improved along the decades thanks to the growing number of contributing observatories spread around the world. In this contest, an important contribution comes from the observations collected from remote and inaccessible areas, as those from the polar regions where the field is stronger than in any other place, its geometric dipolar pattern shows high space gradients and asymmetric spatial features and temporal variations are also present. The Earth's magnetic poles (also known as vertical or dip poles), defined as the points where the horizontal component of the field vanishes, are located in polar areas; they are not coincident with the geomagnetic (analytic) poles nor the poles of rotation of the Earth (geographic poles) as discovered during the epic voyages of the past centuries.

The famous captain James Ross was the first person who located the north magnetic pole in 1831 at 70° 05′ N, 96° 46′ W (Ross, 1834). Following determinations culminated in the last published location by Newitt et al. (2009) at 83° 57′ N, 120° 43′ W in 2007, as an average results from different analyses based on ground measurements. A detailed list of past determinations derived from ground measurement is also published in Newitt et al. (2009).

Direct measurements of the south magnetic pole location started later than those of the north hemisphere, since Antarctic continent is more difficult to reach, being surrounded by the most stormy seas of the world, contrarily from the Arctic which is surrounded by inhabited lands. The first reliable surveys are dated back to 1899 by Bernacchi and Colbeck (Bernacchi, 1901); later, in 1909, Mawson, David and Mackay (McGregor et al., 1982) stated the first precise location of the south magnetic pole at 72° 25′ S, 155° 16′ E. Few upgrading measurements took place along the 20th century, and the latest observation put the pole at 64°

40′ S, 139° 01′ E in 2000 (Barton, 2002). In summary, simple outcomes from such measurements suggest that magnetic poles are not antipodal and they move along time with different speed rates and patterns, having covered distances of approximately 1,000 km in the last 120 years. An interesting dissertation about the asymmetric behavior of the magnetic dip poles can be found in Mandea and Dormy (2003) and Korte and Mandea (2008); they also show that in the north hemisphere the dip pole has been migrating in the north-western direction, from north Canadian territories toward Siberia, while in the south hemisphere the dip pole has been moving westward. Conversely, the geomagnetic poles, which are derived from the first three terms of the spherical harmonic analysis of the Earth's magnetic field, show to be almost stationary (Thébault et al., 2015).

The independent behavior of the magnetic poles is a reflection of the secular variation of the Earth's internal (core) field, which is the main source of the whole geomagnetic field. On the Earth' surface every measurement contains the contribution from the core field plus the smaller in magnitude crustal and external field, which cannot be separated in the experimental data (Newitt et al., 2009). Nor the models, even the most sophisticated, can perfectly reach the goal since they are based on observations "contaminated" at the source, not to say that their reliability critically depends on the distribution of observational points, still unbalanced because of their scarce presence in polar areas and open oceans. Nevertheless, in models based on spherical harmonic expansions, choosing the right combination of the order and degree of their coefficients and isolating contributions from dipolar and non-dipolar origin, some aspects of the separation between internal and external contributions to the geomagnetic field can be explained but some others need to be further modeled and investigated. Indeed, considering not only the centered magnetic dipole but also the eccentric dipole and higher order terms, the presence of the geomagnetic poles and of the dip poles, together with their not-antipodal characteristics, may be well distinguished as described by Fraser-Smith (1987). At time scales shorter than 1 year, even the contribution from external sources (magnetospheric and ionospheric currents) is needed to explain the short time dip poles displacements, such as their cyclic diurnal paths (Dawson & Newitt, 1982).

Among the group of "pole" family, (geomagnetic, eccentric, geographic, pole of inaccessibility, etc.) the dip poles are the unique poles which can be located by means of direct experimental measurements which remain, in principle, superior of any response from any model, rather they contribute to test and increase the accuracy of global and regional models, especially in polar regions. The fascinating topic about the nature of the Earth' magnetic field and its main features, like the ones related to the displacement and velocity of the north and south dip poles, attracts the curiosity of the general public and, hopefully, a new generation of students. The attractive possibility to use observational satellite data, benefiting from their lifetime and huge data production, allows to monitor the position and motion of such poles through month-by-month analysis using physical measurements (and later through models which require long times to be released) and helps to keep the interest on these topics alive. The time-space evolution of the dip poles, which is an independent parameter reflecting the existence of internal processes of our planet, should foster the investigation of scientists belonging to different domains of knowledge than Earth's magnetism. As in the past through the Ørsted (Hulot et al., 2002) satellite mission, which provided an improvement in the knowledge of the Earth magnetic field, nowadays we rely on the ESA's (European Space Agency) three Swarm satellites, coded as Alpha (A), Bravo (B) and Charlie (C), provide a huge amount of data, allowing us to overcome at once the criticisms of deriving the dip pole positions from ground-level surveys (Campbell, 2003):

- From few spot measurements (weak statistics)
- Inevitably under unpredictable magnetic external conditions during scheduled and time-limited surveys
- With contamination by crustal unwanted contributions

Ground surveys in polar remote regions cover a limited and well definite area, have a short duration and need to be planned in advance with big logistics efforts, no matter the possible sudden change of the external forcing conditions leading to less reliable results.

On the contrary, Swarm satellite mission provides a continuous and progressively longer data set, collecting data at different global magnetic conditions (quiet, moderate and disturbed). Moreover, at the satellite altitudes crustal small scale wavelength structures give very weak contributions to the field recorded by onboard equipment. Obviously the external contributions are present in Swarm measurements and can trigger

a short term variability of the dip poles position; this feature can be an advantage in studying the Sun-Earth relations; however, in our case it can be disregarded since we are focusing on the long term dip poles variability and averaging procedures imply that the external contributions are negligible.

In a previous paper, based on the data set from Swarm A and B, Jan 2014–Apr 2016, the dip poles positions and their spatial shift under different geomagnetic conditions were estimated (Lepidi et al., 2018). In this paper, we use a larger data set, from Swarm A, B and C, during years 2015–2019, in order to establish a robust mathematical method for determining the dip poles positions and their long term displacement in the analyzed time interval. Years 2015–2019 mark the descending phase of solar cycle 24, spanning from high-moderate to low level of solar activity. The dip poles positions found from Swarm data are also compared with the ones derived from the last generations of the International Geomagnetic Reference Field (IGRF) model. Its 12th generation (IGRF12, Thébault et al. (2015), https://www.ngdc.noaa.gov/IAGA/vmod/coeffs/igrf12coeffs.txt) was released in 2015, and so its results for 2015, relying on updated geomagnetic data for that year, are the best ones to which Swarm data set can be compared. A further opportunity, was given us by the latest IGRF release: the 13th generation of the model (IGRF13, https://www.ngdc.noaa.gov/IAGA/vmod/coeffs/igrf13coeffs.txt), dated on December 2019, which allows a further comparison, being more reliable for years 2016–2019, which are not any more resulting from extrapolated predictions as they were for IGRF12. The long-term variation of the Earth's magnetic field is a topic of current deep scientific importance for terrestrial physics. The monitoring of the intriguing different behavior of south and north dip poles, especially evident in their mutable positions and velocities along the years, may contribute to the knowledge of the mechanisms that are fundamental in the generation of the Earth's magnetic field. Current availability of satellite datasets allows us to determine in short time (within months) the dip poles positions and their displacements. Once verified that experimental data from satellite equipment are statistically consistent with those from the traditional ground-based geomagnetic observatories through global models but with some limitations better explained in the next sections, we prove the advantages of a prompt knowledge of the pole positions without the need for global models to be released (typically every 5 years).

2. Data and Methods

Swarm satellite constellation consists of three satellites in polar orbit; each of them orbits 15 times in a day (about 95 min per orbit) and in one second covers about 8 km, corresponding to a latitudinal amplitude $\delta\lambda$ ~0.072°. We use Swarm A, B and C magnetic field measurements provided by three-axis stabilized vector field magnetometers (VFM) at 1 s sampling rate and projected in the North-East-Center (NEC) geocentric reference frame. For each sample and for each satellite, also geocentric radial distance r, latitude λ, and longitude ϕ are provided. Swarm mission started on November 22, 2013 and all satellites reached stabilized altitudes approximately in May 2014 (https://earth.esa.int/web/guest/missions/esa-operational-eo-missions/swarm/data-access/orbit-instrument-availability): Swarm A and C fly in a tandem configuration at altitude h of ~450 km (considering $h = 0$ at the standard average Earth's radius), while Swarm B, which is azimuthally shifted with respect to Swarm A and C, at ~530 km. Actually, all these altitude values are referred to 2014 and decrease with increasing time at a rate of ~0.1 km/month (B) and ~0.3–0.6 km/month (A and C) during 2014–2019. For further details on the Swarm satellite instruments visit https://earth.esa.int/web/guest/missions/esa-eo-missions/swarm/instruments-overview; see also Merayo et al. (2008), Qamili et al. (2018), Tøffner-Clausen et al. (2016), and references therein. The Swarm satellite data set is subject to reprocessing procedure leading to progressive releases from the ESA team when their improved quality is reached (e.g., removing systematic noise). For this reason, we use data available at the ESA data portal since September 2019. We are interested in estimating the dip pole location at a given time and reliable altitude, and so to minimize the effect of progressive magnetic poles displacement and decrease of spacecraft orbital altitudes we analyze magnetic field measurements by considering 1-year time intervals; each interval is centered at January 1st of each year from 2015-2019; within a year, the maximum altitude deviation with respect to its central value is about 0.7% for Swarm A and C and about 0.1% for Swarm B. The dip pole identification procedure can be subdivided in two different sub-procedures: the subset selection and the regional modeling scheme. These procedures are separately described in the following subsections.

2.1. The Subset Selection

The generation of a subset of our target data can be summarized as:

1. The original time series are magnetic field measurements at 1 Hz sampling rate in the NEC reference frame, that is, consisting in B_N, B_E and B_C components. In the present analysis, we do not use the B_C component
2. The magnetic field measurements are grouped into a regular grid identified by λ and ϕ distinct intervals, separately for the south and north hemisphere
3. For each grid cell, the average values $\overline{B}_N$ and $\overline{B}_E$ and their variances σ_N and σ_E are computed from data which are in the range 20%–80% of the empirical cumulative distribution function, independently for the three Swarm satellites; each average value is attributed to the center of the corresponding grid cell. Each cell is also associated to its number of data, that is, to its degrees of freedom (DoF)

For obtaining reliable and significant results, the choice of the grid, that is, of the cell dimension $\Delta\lambda$ and $\Delta\phi$, is fundamental to get the appropriate balance between the need of a good spatial resolution and a significant DoF in each cell. In this regard, we use a grid resolution of ∼0.4° in both directions. The average magnetic field components computed with the procedure described above will be hereafter indicated as Swarm subset; we have a different subset for each satellite and for each year.

An example of the horizontal magnetic field $H = \sqrt{\overline{B}_N^2 + \overline{B}_E^2}$, computed by using Swarm A 2015 data, is shown in Figure 1 for the north (panel a) and south (panel b) hemisphere. The standard deviations of the horizontal field $\sigma_H = \sqrt{\sigma_N^2 + \sigma_E^2}$, normalized to the average H, are also shown in panels (c) and (d). Overall availability of data falling in each cell (DoF) contributing to the Swarm subset for both hemispheres can be seen in panels (e) and (f). Circular gaps around the north and south geographic poles in all panels correspond to the areas uncovered by Swarm A satellite, whose orbits do not pass over them. Similar features are obtained for the other two satellites, Swarm B and C (not shown here).

2.2. The Regional Modeling Schemes

The location of each magnetic pole could be, in principle, identified as the minimum of the horizontal field from Swarm subset above computed. However, each ensemble linked to a specific cell is a result of the history of the geomagnetic activity and its associated average magnetic field could be higher/lower than from the other nearest ensembles due to statistical fluctuations. In addition, the possible selection of particular geomagnetic activity conditions would reduce the DoF and the reliability of the averages, leading to spatial gaps in the extreme cases. Moreover, the dip pole position, estimated as the minimum of H in experimental data, is subject to the spatial resolution determined by the grid dimension that can be made smaller at the cost of a weaker statistics.

We retain that the dip poles position should be better identified by using an appropriated analytic model on the satellite data subset. Several regional analytical methods were historically adopted for this purpose: the spherical cap harmonic analysis (SCHA; Haines [1985]; Haines [1988]) and two-dimensional Taylor polynomial (TP) fit (e.g., Meloni et al. (1994); Newitt et al. (2009)). Although the SCHA should be better in principle for a data set over a sphere, guaranteeing the orthogonality of the harmonic functions, we prefer to use the TP method which is simpler and applicable to regional magnetic field measurements regardless the orthogonality of the base functions, conversely required by SCHA approach. Moreover, the TP fit can be used also when the number of observations is limited, that is, when the SCHA could lead to unstable solutions (see, e.g., Newitt et al. (2009)), then allowing to conduct also short term analyses or analyses under particular conditions.

The modeling scheme can be summarized as it follows:

1. Regional analysis by means of a polynomial model implies to restrict the spatial domain to have a better convergence of the fit procedure. Therefore, we numerically identify the minimum value of the horizontal component of the magnetic field H and its coordinates (λ_0, ϕ_0) and then restrict our investigation to the region $\lambda_0 \pm 10°$ and $\phi_0 \pm 10°$. The dip poles motion rates at short time scale (Dawson & Newitt, 1982) guarantee that the dip poles, within each year, are well inside the chosen regions.

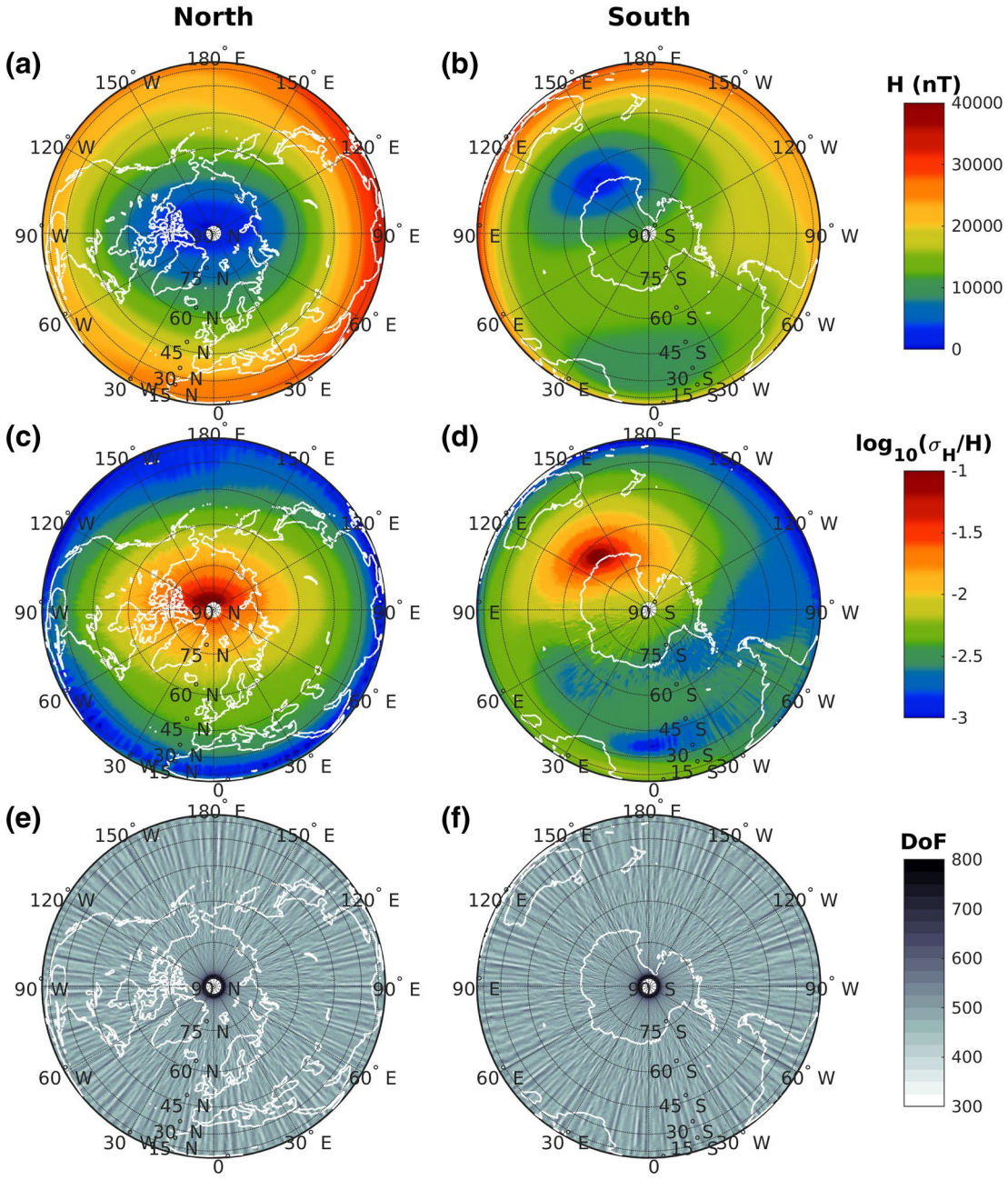

Figure 1. Average horizontal magnetic field H in the north (a) and south (b) hemisphere during year 2015 (Swarm A). The corresponding normalized standard deviations σ_H/H are shown in panels (c) and (d), while the corresponding numbers of 1 Hz data (degrees of freedom, DoF) are shown in panels (e) and (f). White small circles at the center of each figure are data gaps since the satellite does not cover the small areas just around the geographic poles. Each map is obtained by using an orthographic projection and looking downward to the pole.

2. The squared experimental horizontal field values H^2, one value for each cell of the grid, are fitted by using a TP method of this kind, in order to obtain a modeled field H^2_{mod}

$$H^2_{mod}(\lambda,\phi) = C_0 + \sum_{n=0}^{N}\sum_{m=0}^{M} A_{nm}(\lambda-\lambda_0)^n(\phi-\phi_0)^m \quad (1)$$

where the maximum orders $M = N = 5$ are chosen and the unknown coefficients A_{nm} (n, m = 0,1,2,..,5), are estimated through least square method by using weighted estimations, with weights represented by

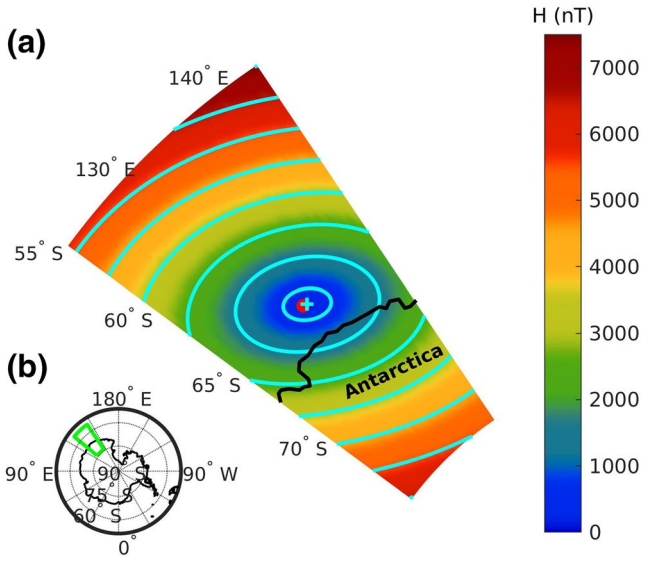

Figure 2. An example of the application of the Taylor polynomial (TP) fit to determine the south magnetic pole from Swarm A subset during 2015. The horizontal field (H) is shown in color scheme (panel a), while the light blue lines mark the intensity levels of the modeled field (H_{mod}). The dip pole determined as the minimum of horizontal field (red dot) and that estimated by using the TP fit (light blue cross) are also indicated. The Antarctic sector shown in panel (a) is highlighted in panel (b) with green contour.

DoF; λ_0 and ϕ_0 represent the origin of expansion, while C_0 is introduced to set the minimum value of H_{mod} to zero.

3. We identify the reliable dip pole location by estimating the minimum value of the horizontal field modeled by TP fit (H_{mod}). For this purpose, we use a grid with a resolution at least 20 times higher than that used to compute the Swarm subset, which corresponds to an angular resolution of 0.02° (~2.4 km at approximate average satellite altitude of 450 km).

Regional modeling described above requires the area of interest to be small enough in order to guarantee that a plane approximation holds and, at the same time, large enough to contain a reasonable number of data samples and to reduce in the core area the effect of possible instabilities at the edge of the spatial domain (Newitt et al., 2009). Figure 2 shows an example of the south dip pole identification procedure based on the TP fit above described, by using 2015 Swarm A subset. In this example, the rectangular grid is defined by $\phi_0 \sim 135.8°$ E $\pm 10°$ and $\lambda_0 \sim -64.4°$ N $\pm 10°$ (as previously explained, $\phi_0 = 135.8°$ E and $\lambda_0 = 64.4°$ N are the coordinates of the grid cell where the experimental H minimizes). The cell extension has been properly chosen to be quite symmetric with respect to the field geometry to guarantee a good convergence of the TP fit. It can be seen that H levels of Swarm A subset (in color scheme) match very closely with those represented by TP fit whose intensity levels, with 1,000 nT spacing, are shown as light blue curves which are well approximated by ellipses. It is clear that the pole position identified as minimum of H (red dot) is not coincident with the center of the lower H level where the minimum of H_{mod} is found (light blue cross): a distance between these two minima of ~22 km is found, probably due to uncertainty induced by grid resolution and statistical fluctuations. We can definitely state that considering the minimum of the modeled field leads to a significant improvement with respect to considering simply the minimum of the experimental data, in that the light blue cross better indicates the center of the color contours.

As shown in Figure 1, the north magnetic pole is closer to the geographic one and to the corresponding data gap with respect to the south one. Since Equation 1 describes a function that is not continuous in correspondence of the geographic pole, which represents the singularity of the spherical coordinates, it is clear that TP fit method in geographic coordinates is not easily applicable to the north hemisphere, as we verified in a separated analysis not shown here. This limitation will be easily mitigated by using an appropriated reference frame; the problem indeed could be solved by using a spherical cap-centered reference frame (see for example Haines [1988]), defining the new coordinate axes such that the z axis is far from the geographic pole. In our case, this corresponds to choose a new x axis that passes through the point P(λ_0, ϕ_0), as described in A. Practically, this consists in a rotation procedure from the geographical Cartesian coordinates to the cap-centered reference ones, by defining the origin of Equation 1 as P (λ_0, ϕ_0) that identifies the new x axis. In this reference frame, Equation 1 is simplified as it follows:

$$H^2_{mod}(\Lambda,\Phi) = C_0^{'} + \sum_{n=1}^{N}\sum_{m=1}^{M} A^{'}_{nm}\Lambda^n\Phi^m \tag{2}$$

where in the cap-reference frame Λ, Φ and $A^{'}_{nm}$, $C_0^{'}$ represents the new coordinates and coefficients, respectively.

The TP method requires a plane approximation, so it cannot be applied to a large region over a sphere. Therefore, on the basis of previous discussion, we set the maximum amplitude of the cap-centered domain to 20°.

In Figure 3, the results obtained from 2015 Swarm A subset by using the cap-centered reference system are shown for both hemispheres. It can be noted that, in both hemispheres, the H intensity levels are not

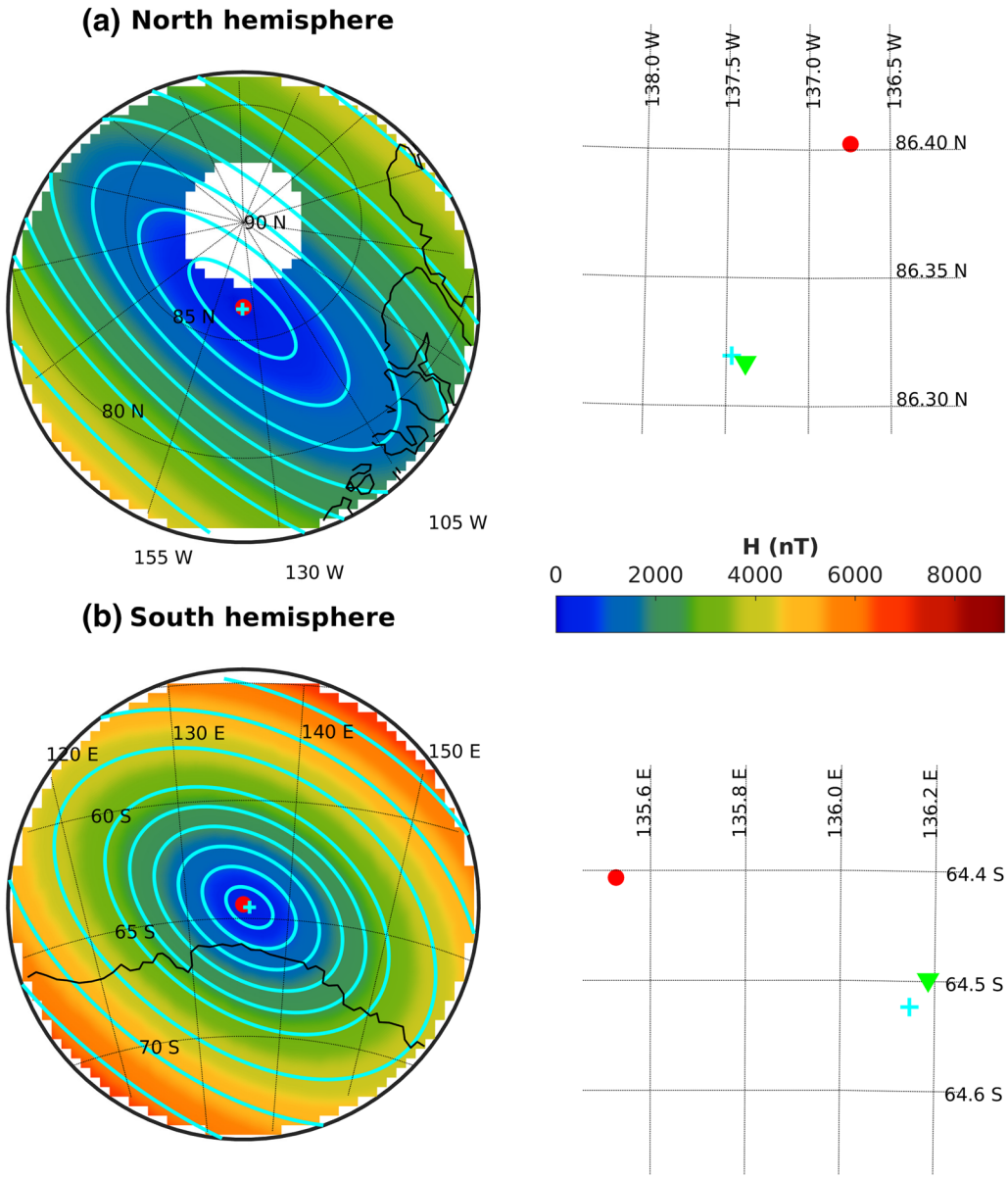

Figure 3. Left panels: the same of Figure 2 obtained using cap-centered reference system for the north (a) and south (b) hemisphere; the horizontal field (H) from Swarm A subset during 2015 is shown in color scale; intensity levels of *H* computed by means of the Taylor polynomial (TP) fit are marked as light blue lines. The dip poles found by TP method are shown by light blue crosses and the ones determined as the minimum of horizontal field are shown by red dots. Right panels: a zoom of the area around poles where also the International Geomagnetic Reference Field (IGRF13) dip poles are shown by green triangles.

circles (as expected for a dipole field) but ellipses, with a greater eccentricity (i.e., the ratio between the major and minor axis of the ellipse) around the north with respect to the south magnetic pole. This feature clearly indicates the presence of a non-dipole field contribution, more evident in the north hemisphere. The distance between the dip poles from TP fit (light blue crosses) and the ones determined as the minimum of the horizontal field (red dots), using an average satellite altitude of ~450 km, are ~11 km and 35 km in the north and south hemisphere, respectively. In the right panels of Figure 3 we show a zoom of the area around the dip poles, where also the ones from IGRF13 model (green triangles) are reported, computed using the iterative procedure described in the following Section 3.1 and referred to the approximate average satellite altitude. It is evident that the dip poles from TP fit are very close to the ones from the model (the distances

are ∼1 and ∼4 km in the north and south hemisphere, respectively), differently from the ones determined as horizontal component minimum.

3. The Dip Pole Positions During 2015–2019 Observed by Swarm Satellites

The TP method is used to identify a reliable dip pole position in both hemispheres for years from 2015 to 2019. However, before applying it to the experimental Swarm data and showing the results, it is important to test the reliability and possible limitations of the method. The present section is then subdivided in two distinct subsections. In the first one, the TP method is applied to geomagnetic field data from a numerical model of the Earth's magnetic field, to check its efficiency, while in the second one the method is used for the identification of the dip pole positions in both hemispheres using geomagnetic field data from Swarm satellites.

3.1. Reliability and Efficiency of TP Method

In this section, we investigate the reliability of TP method. For this purpose, we use, separately, both IGRF12 and IGRF13 models; obviously, since our purpose is just to test a mathematical method, the use of the two models should be perfectly equivalent.

The magnetic poles derived from IGRF, hereafter indicated as IGRF-dip poles, are identified by the following iterative procedure, independently applied to both hemispheres and both IGRF models:

- We define, at the first step, a regularly spaced grid and we calculate for each cell of the grid the IGRF H value at the center. We use, as initial IGRF-dip pole coordinates, the cell where the horizontal IGRF field minimizes
- Then, we iteratively increase the grid resolution around the minimum from previous iteration, and we consequently identify a more reliable IGRF-dip pole position
- The procedure continues until the coordinates of the IGRF dip pole are stable within 10^{-2} km.

For this procedure, we use a cap-centered reference frame, centered around the horizontal IGRF field initial minimum. The January 1, of each year is chosen as center of the 1-year time interval for IGRF-dip pole estimation, consistently with the procedure for computing the Swarm subset. Since, our final purpose is to estimate the dip pole position from Swarm satellites, also in this test procedure based on IGRF model data we conveniently use the geocentric (not geodetic) reference frame at the average satellite altitude h_0 computed over each year in each hemisphere.

For outlining both the uncertainty and reliability of the TP method, we perform a Monte Carlo (MC) test based on Q iterations as it follows:

- B_N an B_E components of the geomagnetic field are computed, over the same Swarm subset grid, from IGRF model and, at each iteration, the deviations $\eta_N\sigma_N$ and $\eta_E\sigma_E$ are added to the B_N an B_E values, leading to the horizontal component deviated data set

$$\hat{H}^2 = (B_N + \eta_N\sigma_N)^2 + (B_E + \eta_E\sigma_E)^2 \tag{3}$$

- where σ_N and σ_E are the standard deviations of the satellite data over the corresponding grid cell and year, and η_N and η_E are random coefficients uniformly distributed in the range $[-1,1]$
- The TP method is applied to the $\hat{H}$ data set, estimating the coordinates of the dip pole, which in principle could be dislocated with respect to those of the modeled IGRF-dip pole
- The procedure is iterated Q times, producing a set of Q-dip pole coordinates.

MC test requires an assigned number Q of iterations, or runs, following the concept that the higher the Q value, the better the estimation of the coordinates. However, for a practical purpose, it is useful to determine an optimum value of Q.

By considering the dip pole coordinates evaluated from each MC run as a random variable, function of Q, we study the convergence of MC test to a stable solution. For this purpose, we perform 50 independent MC tests for $Q = 10$, 50, 100, 500, and 1,000 and, for each Q, we compute the average coordinates $\overline{\lambda}$ and $\overline{\phi}$ and their standard deviations Δ_λ and Δ_ϕ; the latter quantities are fundamental to determine the MC convergence.

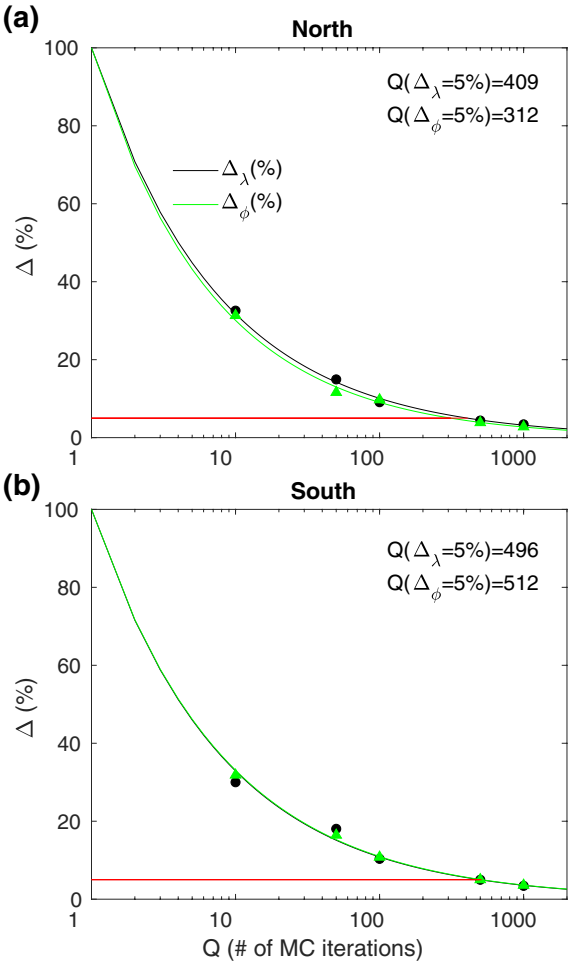

Figure 4. The convergence of Monte Carlo (MC) test. The normalized standard deviation Δ(%) on 50 independent MC tests with 10, 50, 100, 500, and 1,000 iterations, for the north (a) and south (b) hemisphere are shown. The results for the latitudes (black dots) and longitudes (green triangles) are well fitted by an exponential law (solid lines). The red straight lines indicate the $\Delta = 5\%$ value whose corresponding numbers Q (Δ) are also reported.

Figure 4 shows the dependence of the normalized $\Delta_\lambda(\%)$ and $\Delta_\phi(\%)$ on the number of MC iterations Q. It is clear the decrease of Δ for increasing Q, indicating that MC method converges to a common solution for high Q values. In particular, from the MC convergence test, a reduction greater than 95% in the normalized standard deviations is observed for $Q > 500$ for both hemispheres. Moreover, the examined MC convergence is well represented by an exponential law, which clearly suggests us that $Q \sim$ 1,000 is a reasonable value in order to obtain Δ values well below 5%. In this figure, the MC test is applied to IGRF12; from IGRF13 equivalent results (not shown here) are obtained.

Figure 5 shows the MC test results obtained by using TP method to synthetically modified IGRF12 and IGRF13 datasets and by using $Q = 1{,}000$ iterations. The dip pole coordinates estimated through this test for the north and south hemisphere, together with their standard deviations, are compared with the corresponding IGRF-dip poles coordinates. It can be seen that dip poles from IGRF and those from TP method applied to randomized IGRF data are comparable, with maximum differences of few kilometers in the north hemisphere and even smaller in the south one. In any case, the IGRF-dip poles are well within the MC estimated dip poles confidence intervals. The differences between IGRF models results will be discussed in the following sections.

In the above described procedure, the TP method is applied to IGRF data computed at altitude h_0 and deviated with σ_N and σ_E, where h_0, σ_N, and σ_E are from Swarm A satellite; the procedure is also repeated by using Swarm B and C and results (not shown here) are consistent with those obtained for Swarm A, clearly testifying the reliability of the TP method.

3.2. Dip Poles Identified by Using the TP Method on Swarm Satellites Data

In this section, we show the resulting dip poles positions estimated in the cap-centered reference frame with the TP method applied to Swarm satellites data. For comparison, we also estimate the dip poles through both IGRF 12 and 13 models applied to the same cap-centered grid used for estimating TP dip poles from Swarm data.

It is useful to calculate the confidence intervals for the estimated dip poles coordinates, $\lambda_\pm$ and $\phi_\pm$. By using $\overline{B}_N$, $\overline{B}_E$, σ_N and σ_E from satellite subset, we compute the upper/lower $H_\pm^2$ as it follows

$$H_\pm^2 = (\overline{B}_N \pm \sigma_N)^2 + (\overline{B}_E \pm \sigma_E)^2 \tag{4}$$

and we estimate the dip poles coordinates confidence bounds by applying the TP fit to $H_\pm^2$.

In Figures 6 and 7, we show the dip poles coordinates estimated by TP method for Swarm A and B, respectively, and their confidence intervals (red), together with the dip poles coordinates estimated using IGRF12 (black) and IGRF13 (green) models at the average satellite altitudes for each year of the interval 2015–2019. Swarm C results are not shown since they are practically the same as those of Swarm (A).

It can be seen a general good correspondence between experimental and model dip poles coordinates time series; indeed, the correlation coefficients attain values at least of 0.98, where the 95% correlation threshold from null-hypothesis of uncorrelated five points is ∼0.88. The highest correspondences with both models are found for all the considered years in the south hemisphere, where the two IGRF models give similar results and the differences between the TP and both IGRF poles are very small, well within the confidence

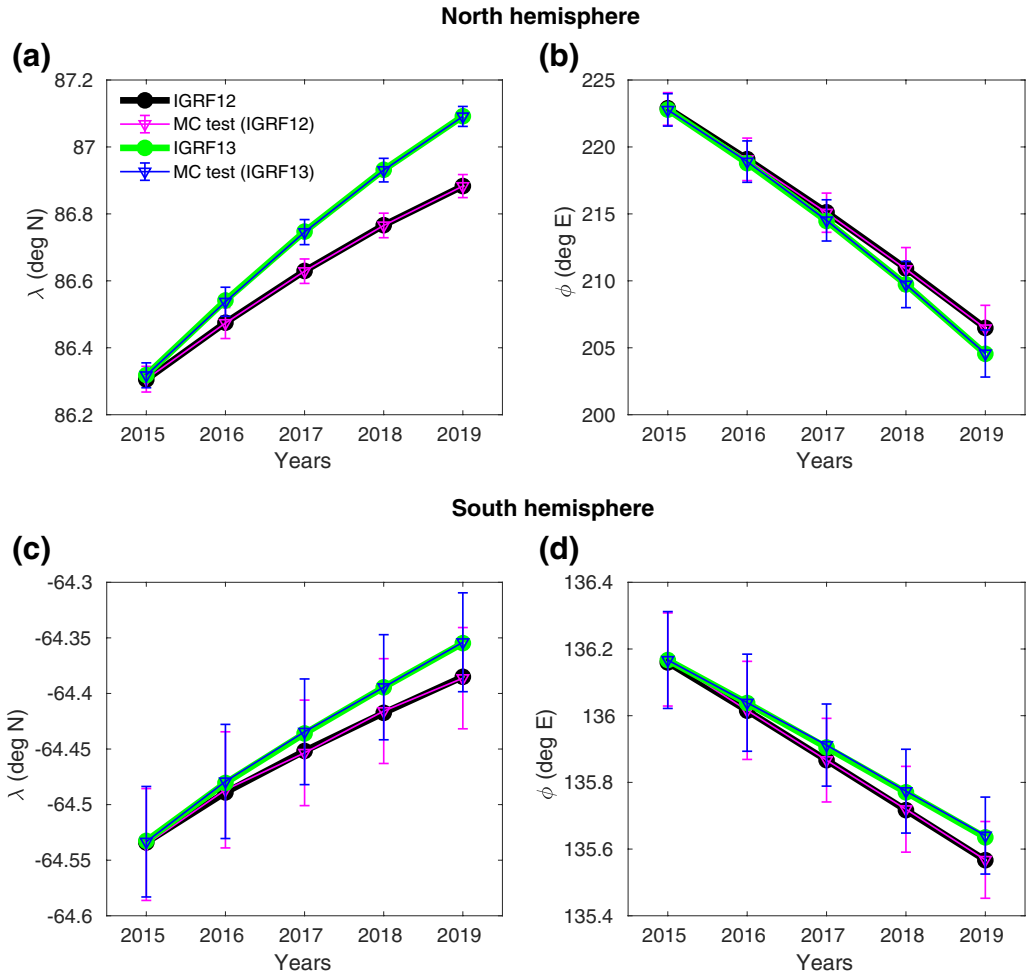

Figure 5. Consistency Monte Carlo (MC) test of Taylor polynomial (TP) method for the identification of the dip poles based on 1,000 iterations. The dip pole coordinates (λ, ϕ) from synthetically modified IGRF data set (see text for details), together with their standard deviations are compared with the International Geomagnetic Reference Field (IGRF)-dip poles for the north (a–b) and south (c–d) hemisphere, for the 2015–2019 time interval.

interval. Conversely, in the north hemisphere for years 2016–2019 a significant difference between IGRF12 and IGRF13 emerges and this allows to state that experimental data better agree with the latest model release. The highest coincidence between dip-poles coordinates from Swarm, IGRF12 and IGRF13 is reached in both hemispheres for year 2015, when IGRF12 was released and both models rely on geomagnetic data, being consequently more reliable. The main difference between the two models emerges for 2016–2019 north dip pole latitudes, with IGRF13 model better following experimental results from Swarm data with respect to IGRF12. For this reason, hereafter we use the IGRF13 model.

Tables 1 and 2 report the dip pole coordinates estimated by TP method applied to all satellites data for the north and south hemisphere, respectively, together with yearly average satellites altitudes. For simplicity, in these tables we report the errors $\Delta\lambda$ (and similarly $\Delta\phi$) calculated as $\Delta\lambda = 1/2\left[(\hat{\lambda}-\lambda_+)^2 + (\hat{\lambda}-\lambda_-)^2\right]^{1/2}$, where $\hat{\lambda} = 1/2(\lambda_+ + \lambda_-)$ indicates the central value of the interval. It is clear how Swarm A and C sense the same dip poles positions, with slight differences in the longitude of the south hemisphere; moreover, it is also clear that the satellites altitudes h progressively decrease along the growing years as stated in Section 2.

We can note from the tables that the dip poles coordinate from Swarm A and C are the same but are slightly different than those from Swarm B which is at a greater altitude; this difference is particularly evident in the north dip pole longitude.

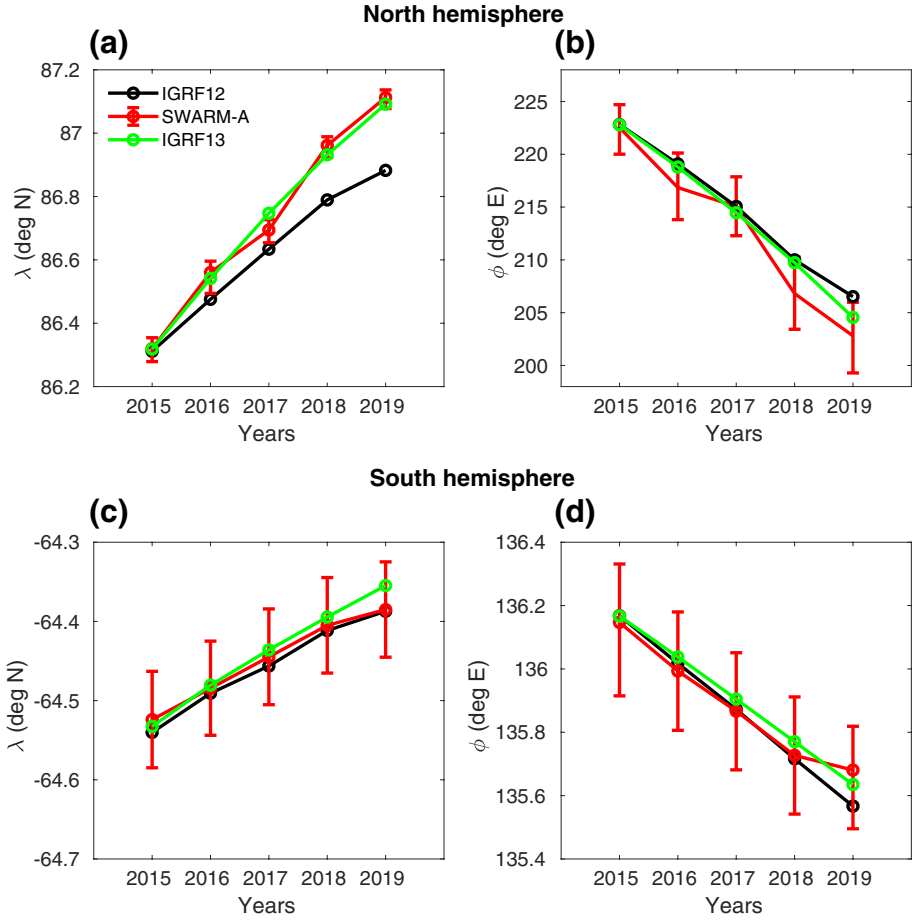

Figure 6. Dip poles coordinates by using Taylor polynomial (TP) method on Swarm A subset (red circles), together with their confidence intervals (red bars), and those estimated by using IGRF12 (black circles) and IGRF13 (green circles) models at average satellite altitude for the north (a–b) and south (c–d) hemisphere are shown.

This is due to the geomagnetic anomalies contribution to the Earth's magnetic field, whose potential is analytically represented by Gauss coefficients g_n^m and h_n^m of degree n greater than 2 of the spherical harmonic expansion of the main geomagnetic field and whose decrease with increasing altitude is sharper than that of the dipolar field.

Making more clear this aspect, we computed the geocentric altitude dependence of the IGRF13 dip poles coordinates obtained taking maximum order of spherical harmonic expansion of the geomagnetic field and following the iterative procedure explained at the beginning of Section 3.1. The results are shown in Figure 8 in both hemispheres for years between 2015 and 2019 (solid blue and magenta lines, respectively). These 2 years are the first and the last one of the analyzed time interval; results for intermediate years (not shown) lie, quite regularly spaced, between them.

We can note an altitude dependence of the IGRF dip pole coordinates: up to approximately 1,000 km, both IGRF dip poles move slightly poleward; moreover, the north one moves eastward and the south one moves slightly westward. Our observations are in good agreement with those obtained by Korte and Mandea (2008) using different models of the main magnetic field. In particular, near Earth's surface the variation with altitude of the location of the north dip pole, especially of its longitude, is stronger than that of the south one. From the figure, it can be also seen the good agreement between the dip poles coordinates from Swarm A and B data (green circles and black crosses, respectively) and the IGRF coordinates at the corresponding altitude and year.

Figure 8 also shows the geomagnetic poles coordinates estimated as the altitude invariant reference point (red dashed lines and circles) which do not change with changing altitude. On the contrary, the coordinates

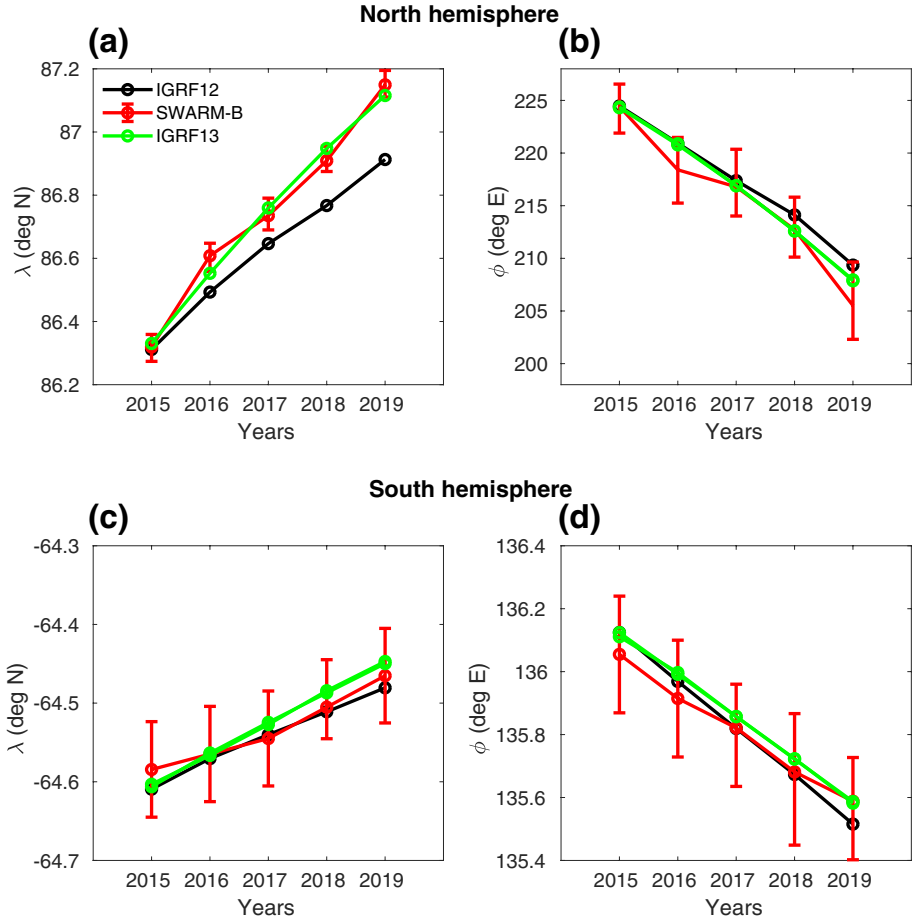

Figure 7. The same of Figure 6 for Swarm B subset.

of dip poles (blue and magenta solid lines) are affected by magnetic anomalies for altitudes up to 10^5 km. Conversely, for higher altitudes ($\sim$ 100 Re) the effects of geomagnetic anomalies vanish and the IGRF dip poles coordinates attain asymptotic values represented by geomagnetic pole coordinates.

For practical purposes, it is important to know the magnetic poles coordinates at ground level. We extrapolate Swarm dip poles positions to $h = 0$ using the altitude dependence found from IGRF13 in the geocentric reference frame. For this purpose, some considerations should be highlighted: (1) the magnetic poles from Swarm data do not exactly coincide with those evaluated from IGRF model at the corresponding altitude; (2) the Earth surface significantly deviates from the spherical shape in correspondence of polar areas. In this regard, we perform the following procedure:

- The altitude dependence used for extrapolating the dip pole coordinates at ground level for each of the examined years is the one found from IGRF13 for the corresponding year
- For each year, we shift the geodetic altitude dependent coordinates of IGRF13 dip poles to have a perfect agreement with Swarm satellite dip pole coordinates; then, from the resulting curve, we extract the dip pole position at $h = 0$ in the geocentric reference frame
- We convert the dip poles coordinates at $h = 0$ from geocentric to geodetic reference frame; this conversion is applied both to the IGRF13 and to Swarm dip poles positions. For this purpose we use the World Geodetic System 1984 (WGS84, https://earth-info.nga.mil) ellipsoidal reference frame

In order to, have unique dip poles locations at ground level for each year, we compute the averages of the dip pole coordinates from the three Swarm satellites; the resulting values, together with their standard error of the mean, are shown in Table 3. For a comparison, also the IGRF13 dip poles geodetic coordinates are

Table 1
Geocentric North Dip Pole Coordinates at Swarm Satellites Altitudes h and Their Errors Δ, Computed by Using TP method

		TP method to Swarm data						IGRF	
		λ	$\Delta\lambda$	ϕ	$\Delta\phi$	h	Δh	λ	ϕ
Year	Swarm	(deg N)	(deg)	(deg E)	(deg)	(km)	(km)	(deg N)	(deg E)
2015	A	86.32	0.04	222.53	2.35	455.72	8.91	86.32	222.78
	B	86.32	0.04	224.41	2.33	507.71	3.44	86.33	224.33
	C	86.32	0.05	222.53	2.51	455.71	8.90	86.31	222.87
2016	A	86.56	0.05	216.85	3.15	444.52	8.91	86.54	218.90
	B	86.61	0.04	218.41	3.12	502.91	3.44	86.55	220.84
	C	86.56	0.05	216.85	3.18	444.55	8.90	86.54	218.88
2017	A	86.69	0.04	215.05	2.79	438.90	8.91	86.75	214.44
	B	86.74	0.05	216.79	3.17	500.97	3.44	86.75	217.06
	C	86.69	0.04	215.05	2.79	438.90	8.90	86.75	214.43
2018	A	86.96	0.03	206.81	3.42	435.57	8.91	86.93	209.74
	B	86.91	0.04	212.73	2.85	499.86	3.44	86.94	212.72
	C	86.96	0.03	206.81	3.42	435.57	8.90	86.93	209.71
2019	A	87.11	0.03	202.80	3.35	433.23	8.91	87.09	204.50
	B	87.15	0.04	205.51	3.67	499.08	3.44	87.11	208.24
	C	87.11	0.03	202.80	3.35	433.24	8.90	87.09	204.48

Note. Last two columns report the dip poles estimated by IGRF13 model at satellites altitudes.
IGRF, International Geomagnetic Reference Field; TF, Taylor polynomial.

reported. The Swarm and IGRF13 dip poles positions reported in Table 3 are also shown in Figure 9, in orthographic maps as points with error bars; it is evident that both dip poles move in the north-west direction.

From the yearly dip poles positions reported in Tables 1 and 2, extrapolated to $h = 0$, we compute the dip pole velocities for each satellite and, consequently, the yearly average velocities (reported in Table 4), together with their standard error of the mean: for the north hemisphere they attain values between ∼37 km/y and 72 km/y, with the lowest value during year 2016; conversely for the south hemisphere they are between ∼5 km/y and 9 km/y. Note that the different velocity in the two hemispheres is responsible for the larger difference in the north pole position errors as reported in Tables 1 and 2. In fact, their uncertainty can be trivially estimated as $\Delta x = V\Delta t$, where V is the velocity (greater in the north) and Δt is the time interval (1 year).

4. Discussions and Conclusions

The magnetic poles of the Earth are situated in polar areas of both hemispheres, in locations that are difficult to reach for collecting on-site measurements. Furthermore, any occasional ground surveys of data are subject to the external magnetic conditions (ionospheric and magnetospheric environment modifications) which, in turn, may significantly alter the determination of the position of the magnetic poles on the surface of the Earth. Such conditions are unpredictable, making potentially fruitless the attempt to catch the poles; they have inevitably characterized the first epic explorations carried out in the past centuries and are still a heavy limitation even for modern surveys. Nowadays, an important contribution to the measurement of the Earth's magnetic field comes from the satellites missions, in orbit for covering the observations of many parameters. They return a large amount of data, in different magnetic conditions, implicitly overcoming the limitation of reaching harsh areas of the Earth's surface and allowing to achieve reliable results thanks to robust statistics.

This work investigates the possibility to derive the location of the magnetic poles of the Earth from data collected by the ESA's Swarm constellation of three satellites put into orbit at the end of 2013, specifically

Table 2
The Same of Table 1 Referred to the South Hemisphere

		TP method to Swarm data						IGRF	
		λ	$\Delta\lambda$	ϕ	$\Delta\phi$	h	Δh	λ	ϕ
Year	Swarm	(deg N)	(deg)	(deg E)	(deg)	(km)	(km)	(deg N)	(deg E)
2015	A	−64.52	0.06	136.15	0.21	473.92	8.45	−64.53	136.16
	B	−64.58	0.06	136.05	0.19	526.00	3.37	−64.61	136.13
	C	−64.52	0.06	136.13	0.16	473.90	8.48	−64.53	136.17
2016	A	−64.48	0.06	135.99	0.19	462.99	8.45	−64.48	136.03
	B	−64.56	0.06	135.91	0.19	521.28	3.37	−64.57	135.99
	C	−64.48	0.06	135.96	0.18	462.98	8.48	−64.48	136.04
2017	A	−64.44	0.06	135.87	0.18	457.42	8.45	−64.43	135.89
	B	−64.55	0.06	135.82	0.16	519.28	3.37	−64.53	135.87
	C	−64.44	0.06	135.82	0.16	457.43	8.48	−64.44	135.91
2018	A	−64.41	0.06	135.73	0.18	453.98	8.45	−64.40	135.79
	B	−64.51	0.05	135.68	0.21	518.22	3.37	−64.48	135.71
	C	−64.41	0.06	135.73	0.16	453.98	8.48	−64.39	135.77
2019	A	−64.39	0.06	135.68	0.16	451.69	8.45	−64.35	135.64
	B	−64.47	0.06	135.59	0.16	517.41	3.37	−64.45	135.59
	C	−64.39	0.05	135.63	0.16	451.70	8.48	−64.36	135.64

IGRF, International Geomagnetic Reference Field; TF, Taylor polynomial.

equipped with both vector and scalar magnetometers. The almost polar orbits of the three satellites ensure adequate coverage of the polar areas, although a small data gap is systematically present around the geographic poles. In particular, we analyze 5 years (2015–2019) of Swarm satellites data. For each year, Swarm data are averaged over a regular grid covering a spherical cap region and the resulting average field is analyzed to determine the position of the dip poles, defined as the point where the horizontal component of the magnetic field minimizes. Being interested in the yearly location and long term migration of the magnetic poles, within each year we do not apply any selection about time, magnetic activity or external conditions (actually we just exclude data outside the range 20%–80% of the empirical cumulative distribution function), since annual averages cancel the negligible contribution of the daily or even seasonal fluctuations in the position of the poles as well as any displacement related to the magnetospheric and ionospheric dynamics of external origin. For each year, we determine the dip poles coordinates by means of two-dimensional TP fit method, after proving its reliability by using a MC test. A further step, consists in verifying the agreement of the derived locations of both poles with those gathered from the mathematical derived models of the field, such as the IGRF model; we consider both the 12th generation of this model (IGRF12), released in 2015, and the latest version (IGRF13), released in December 2019. Our analysis shows a general good agreement between experimental and model positions; the best agreement is found for 2015, when both IGRF models rely on geomagnetic data and are consequently more reliable than in the following years (2016–2019) when results came from extrapolated (for IGRF12) or interpolated (for IGRF13) projections. For the south hemisphere, results from IGRF12 and IGRF13 models are quite close for the whole 2015–2019 period and both are in good agreement with experimental dip poles positions observed by our study. Conversely, for the north hemisphere during years 2016–2019 the two models provide appreciably different results and IGRF13 better follows the experimental north magnetic pole positions with respect to previous IGRF12 model. We underline that both IGRF models are based on a combination of Swarm, historical satellite data and ground-based observatory data (Olsen et al., 2015).

The positions of the magnetic poles found from Swarm data correspond to the altitude of flight of each satellite; for practical purposes, these positions have to be projected to the ground, for continuing the series

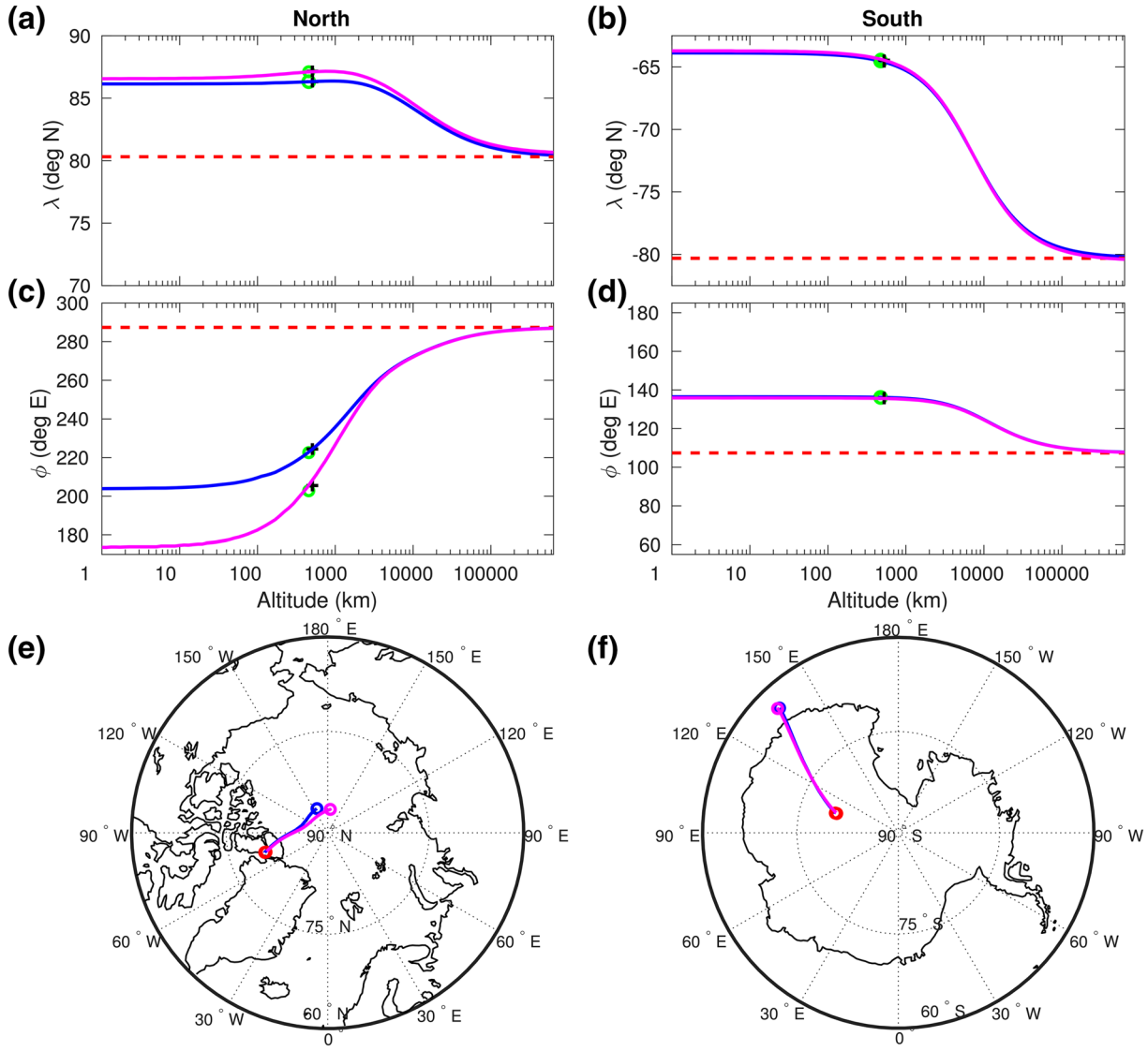

Figure 8. (Panels a–d) The dependence of the dip poles coordinates from IGRF13 model on the geocentric altitude above the Earth surface for 2015 and 2019 (solid blue and magenta lines, respectively) together with the 2015 IGRF13 geomagnetic poles coordinates (dashed red lines; the ones for 2019 are essentially the same). The dip pole positions estimated by Taylor polynomial (TP) method on Swarm A (green circles) and B (black crosses) data are also indicated at corresponding altitudes. (Panels e–f) The altitude dependent International Geomagnetic Reference Field (IGRF) dip pole positions for 2015 and 2019 (in blue and magenta, respectively) projected over orthographic maps. Red circles indicate the geomagnetic poles; blue and magenta circles indicate the IGRF dip poles at ground for 2015 and 2019, respectively.

of the historical recordings made on-site. In this regard, a method to project the dip poles from spacecraft altitudes to the ground, based on the IGRF model, is developed. The resulting geodetic dip poles positions at ground allow us to estimate the dip poles drift velocity: for the north hemisphere it attains values between ~ 37 km/y and 72 km/y, with the lowest values during year 2016, while for the south hemisphere, it is between ~5 km/y and 9 km/y. Interestingly, the observed north dip pole velocity minimum during 2016 could be probably related to the jerk which, according to Aubert and Finlay (2019), occurred in 2016.

Noteworthy considerations can be made from a comparison between the two hemispheres: we can note that in the north hemisphere the field geometry around the magnetic pole has a greater ellipticity with respect to the south hemisphere, where it more closely resembles a circular symmetry; moreover, the north magnetic pole position exhibits a sharper dependence on altitude than the south one. Both these features well agree with findings by Korte and Mandea (2008) based on geomagnetic field models, and seem to indicate a

Table 3
The Geodetic North and South Dip Pole Coordinates at Ground Level Estimated as the Average of Values From the Three Swarm Satellites for Years From 2015 to 2019, Together With Their Standard Error of the Mean (SEM)

	Swarm				IGRF	
	λ	SEM_λ	ϕ	SEM_ϕ	λ	ϕ
Year	deg N	deg	deg E	deg	deg N	deg E
			North magnetic pole			
2015	86.16	0.02	203.72	1.38	86.17	203.71
2016	86.40	0.03	194.52	1.82	86.37	196.49
2017	86.46	0.02	189.30	1.68	86.50	189.06
2018	86.58	0.02	179.28	1.87	86.58	181.16
2019	86.60	0.02	171.66	1.99	86.57	173.40
			South magnetic pole			
2015	−64.01	0.03	136.42	0.11	−64.03	136.47
2016	−63.99	0.03	136.25	0.11	−63.99	136.32
2017	−63.96	0.03	136.12	0.10	−63.94	136.15
2018	−63.92	0.03	135.98	0.11	−63.90	136.02
2019	−63.89	0.03	135.89	0.09	−63.86	135.88

Note. Last two columns report IGRF13 dip poles coordinates at ground level.
IGRF, International Geomagnetic Reference Field; TF, Taylor polynomial.

major presence of crustal contributions to the field in the region around the north magnetic pole, confirming previous results reported in Mandea and Dormy (2003). Moreover, the north magnetic pole during the years moves really faster with respect to the south one, confirming previous results reported in Mandea and Dormy (2003). A possible explanation is that the position and motion of the poles are certainly linked to the core field dynamics and its long-term time variation; however, the two dip poles can be differently free to move, due to the different local field morphology (Korte & Mandea, 2008; Mandea & Dormy, 2003) which is confirmed by our findings. Indeed, as discussed by Thébault (2006), Swarm data can provide an unprecedented capability of detecting lithospheric features both at global and local/regional scale. All these considerations could well explain why the coincidence between Swarm and IGRF13 model magnetic poles positions for years 2016–2019 is slightly worse for the north hemisphere: model results appear to follow with greater difficulty the short scale field features in the area surrounding the north magnetic pole.

We believe that our work can give an important contribution to the almost real-time determination of dip poles positions, going beyond the limits which are intrinsic in the determination of the poles from the IGRF model: the model is based on experimental data for the year of its release, then for this year it can be used to accurately determine the poles positions; however, in the years following the release, its extrapolated projections can track with minor accuracy the poles positions; this is what we have shown to happen for IGRF12, which well indicates the poles positions for 2015, the year of its release, but for 2016–2019 does not follow so closely the north magnetic pole position. Only at the end of 2019, with the latest IGRF13 release, we could check the experimental dip pole positions for years 2016–2019. We are confident that also in future years, before the release of the next IGRF generation, reliable determination of the poles can be obtained by using Swarm data through methods like the one we here propose. The mathematical procedure we describe in this paper, based on the two-dimensional TP fit, focuses on the determination of the minimum of the experimental horizontal component of the magnetic field and not on a complete modelization of the field itself in the surrounding region, as the SCHA does. So this method is easier to be applied also in case of scarcity of experimental data, when the SCHA could lead to unstable solutions (Newitt et al., 2009). In this sense, the method we propose is applicable for determining the magnetic poles positions also for time periods shorter than one year or for selected magnetospheric or solar wind conditions to study the magnetic poles short term dynamics.

Table 4
Yearly Average Velocities at Ground Level of the North and South Dip Poles (V_N and V_S, Respectively), Together With Their Standard Error of the Mean SEM_{V_N} and SEM_{V_S}

North			South	
	V_N	SEM_{V_N}	V_S	SEM_{V_S}
Year	km/y	km/y	km/y	km/y
2015.5	71.4	1.9	8.9	0.5
2016.5	36.8	0.4	7.4	0.7
2017.5	68.9	7.1	8.0	0.5
2018.5	50.6	6.8	5.4	0.8

Note. The first column indicates the center of the time interval over which the average velocities are computed.

Appendix A: Rotation procedure from geographic to cap-centered reference frames

The complete rotation matrix can be generally expressed as product of three elementary rotation matrices around each given axis in the original frame, while, in the Cartesian to cap-centered rotation procedure, two angles are needed: the rotation angle α around the z-axis, which corresponds the new x' and y' axes, and the consequent rotation angle β around the y'-axis, which corresponds the new x'' and z''. By choosing $\alpha = \phi_0$ and $\beta = \lambda_0$, the Cartesian to cap-centered reference frame can be expressed as it follows:

$$R = R_y R_z = \begin{pmatrix} \cos\beta & 0 & \sin\beta \\ 0 & 1 & 0 \\ -\sin\beta & 0 & \cos\beta \end{pmatrix} \begin{pmatrix} \cos\alpha & \sin\alpha & 0 \\ -\sin\alpha & \cos\alpha & 0 \\ 0 & 0 & 1 \end{pmatrix} \quad \text{(A1)}$$

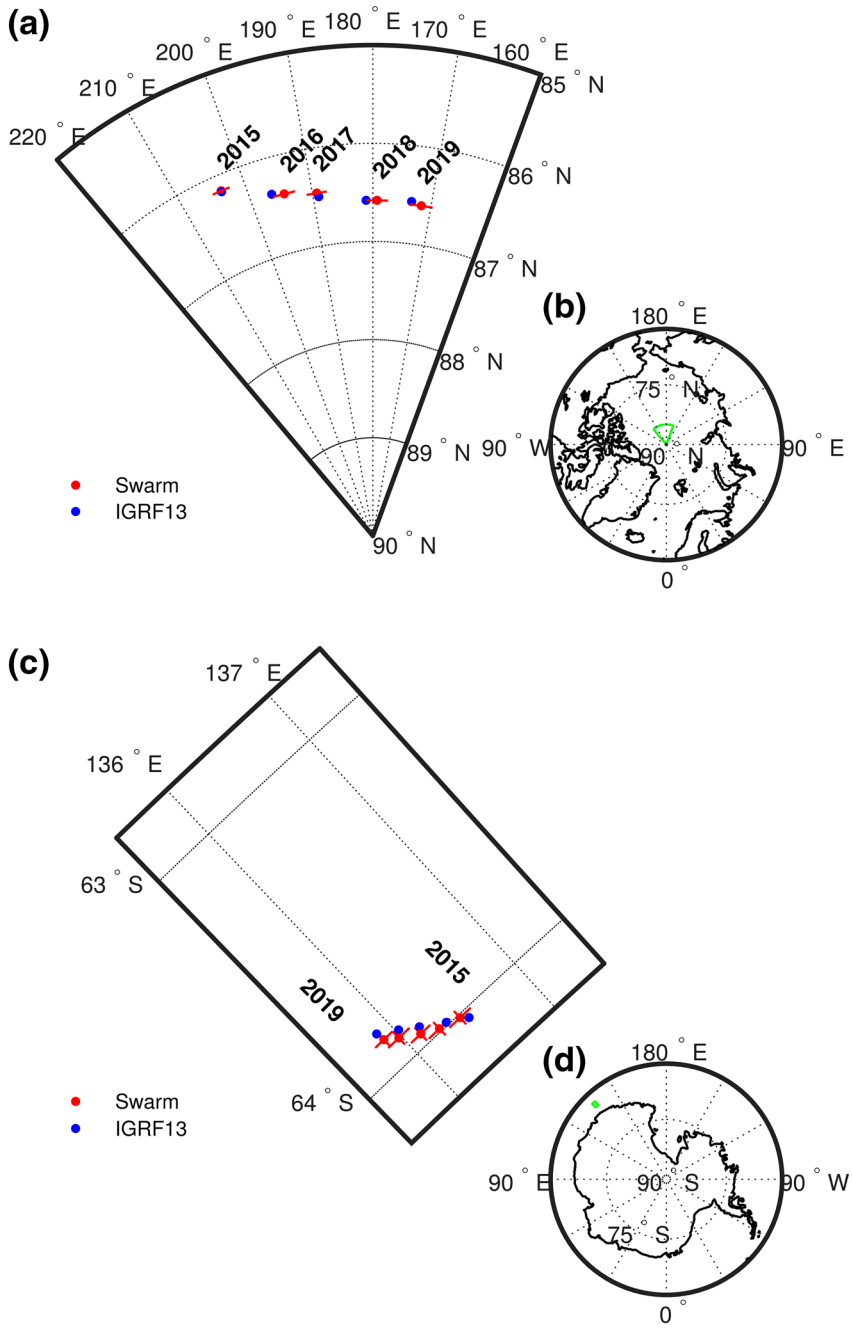

Figure 9. The geodetic Swarm and IGRF13 dip poles positions at ground (red and blue points, respectively) in orthographic maps for the north (a and b panels) and south (c and d panels) hemisphere. The standard errors of the mean are also shown as red bars. The spatial domains shown in panels (a) and (c) are highlighted in panels (b) and (d) with green contours.

In this coordinate system any function of λ and ϕ expandable by means of Taylor two-dimensional function of the form $f(\lambda,\phi) \simeq \sum_{n=0}^{N}\sum_{m=0}^{M} A_{nm}(\lambda-\lambda_0)^n(\phi-\phi_0)^m$ can be simplified as it follows:

$$g(\Lambda,\Phi) \simeq \sum_{N}^{n=1}\sum_{M}^{m=1} A'_{nm}\Lambda^n\Phi^m \tag{A2}$$

With this system it is possible to choose a spherical cap region with the center near the minimum/maximum of the g (Λ, Φ) function, confining any polynomial instability to the periphery of the spherical cap

region. In addition, the symmetry of the spherical cap with respect to the center, near the true pole, makes the resulting fitted quantities reliable.

Acknowledgments
The authors would like to thank all principal investigators and their teams at the European Space Agency (ESA) for providing high quality magnetic data from Swarm satellites, freely available via https://earth.esa.int/web/guest/swarm/data-access. The authors also thank the members of IAGA Working Group V-MOD for computing the IGRF coefficients, freely available at https://www.ngdc.noaa.gov/IAGA/vmod/igrf.html.

References

Aubert, J., & Finlay, C. C. (2019). Geomagnetic jerks and rapid hydromagnetic waves focusing at Earth's core surface. *Nature Geoscience*, *12*(5), 393–398. https://doi.org/10.1038/s41561-019-0355-1

Barton, C. (2002). Survey tracks current position of South Magnetic Pole. *Eos, Transactions American Geophysical Union*, *83*(27), 291. Retrieved from https://agupubs.onlinelibrary.wiley.com/doi/abs/10.1029/2002EO000210

Bernacchi, L. C. (1901). *To the south polar regions: Expedition of 1898-1900.* Hurst and Blackett.

Campbell, W. H. (2003). Comment on "Survey tracks current position of South Magnetic Pole" and "Recent acceleration of the north magnetic pole linked to magnetic jerks". *Eos, Transactions American Geophysical Union*, *84*(5), 40. Retrieved from https://agupubs.onlinelibrary.wiley.com/doi/abs/10.1029/2003EO050008

Dawson, E., & Newitt, L. (1982). The magnetic poles of the earth. *Journal of Geomagnetism and Geoelectricity*, *34*. https://doi.org/10.5636/jgg.34.225

Fraser-Smith, A. C. (1987). Centered and eccentric geomagnetic dipoles and their poles, 1600 - 1985. *Reviews of Geophysics*, *25*(1), 1–16. https://doi.org/10.1029/RG025i001p00001

Haines, G. (1985). Spherical cap harmonic analysis. *Journal of Geophysical Research*, *90*(B3), 2583–2591. https://doi.org/10.1029/JB090iB03p02583

Haines, G. (1988). Computer programs for spherical cap harmonic analysis of potential and general fields. *Computers & Geosciences*, *14*(4), 413–447. https://doi.org/10.1016/0098-3004(88)90027-1

Hulot, G., Eymin, C., Langlais, B., Mandea, M., & Olsen, N. (2002). Small-scale structure of the geodynamo inferred from Oersted and Magsat satellite data. *Nature*, *416*(6881), 620–623. https://doi.org/10.1038/416620a

Korte, M., & Mandea, M. (2008). Magnetic poles and dipole tilt variation over the past decades to millennia. *Earth Planets and Space*, *60*, 937–948. https://doi.org/10.1186/BF03352849

Lepidi, S., Di Mauro, D., Tozzi, R., Cafarella, L., De Michelis, P., & Marzocchetti, M. (2018). Space observations to determine the location of locally vertical geomagnetic field. In C. Foullon & O. E. Malandraki (Eds.), Space weather of the heliosphere: Processes and forecasts (335, p. 135–138). https://doi.org/10.1017/S1743921317007190

Mandea, M., & Dormy, E. (2003). Asymmetric behavior of magnetic dip poles. *Earth Planets and Space*, *55*(3), 153–157. https://doi.org/10.1186/BF03351742

McGregor, P. M., McEwin, A. J., & Dooley, J. C. (1982). Secular motion of the South magnetic. In R. Oliver, J. P. R., & J. Jago (Eds.), *Antarctic earth science* (p. 603–606). Canberra, CBR: Australian Academy of Sciences.

Meloni, A., Battelli, O., Santis, A. D., & Dominici, G. (1994). The 1990.0 magnetic repeat station survey and normal reference fields for Italy. *Annals of Geophysics*, *37*(5). Retrieved from https://www.annalsofgeophysics.eu/index.php/annals/article/view/4185

Merayo, J. M., John, L. J., Friis-Christensen, E., Brauer, P., Primdahl, F., Jørgensen, P. S., et al. (2008). Small satellites for Earth observation. In R. Sandau, H. Roser, & A. Valenzuela (Eds.), *The swarm magnetometry package*. Dordrecht: Springer. https://doi.org/10.1007/978-1-4020-6943-7_13

Newitt, L. R., Chulliat, A., & Orgeval, J. J. (2009). Location of the north magnetic pole in April 2007. *Earth Planets and Space*, *61*(6), 703–710. Retrieved from https://doi.org/10.1186/BF03353178

Olsen, N., Hulot, G., Lesur, V., Finlay, C. C., Beggan, C., Chulliat, A., et al. (2015). The Swarm initial field model for the 2014 geomagnetic field. *Geophysical Research Letters*, *42*(4), 1092–1098. Retrieved from https://agupubs.onlinelibrary.wiley.com/doi/abs/10.1002/2014GL062659

Qamili, E., Tøffner-Clausen, L., Miedzik, J., Bregnhøj Nielsen, J., Vogel, P., & Floberghagen, R. (2018). Swarm magnetic instruments: Status and data quality. In: *Egu general assembly conference abstracts* (p. 8930).

Ross, J. C.. (1834). On the position of the north magnetic pole. *Philosophical Transactions of the Royal Society of London*, *124*, 47–52. Retrieved from http://www.jstor.org/stable/108052

Thébault, E. (2006). Global lithospheric magnetic field modeling by successive regional analysis. *Earth Planets and Space*, *58*, 485–495. https://doi.org/10.1186/BF03351944

Thébault, E., Finlay, C., & Toh, H. (2015). Special issue "International Geomagnetic Reference Field—the twelfth generation". *Earth Planets and Space*, *67*(1), 158. Retrieved from https://doi.org/10.1186/s40623-015-0313-0

Tøffner-Clausen, L., Lesur, V., Olsen, N., & Finlay, C. C. (2016). In-flight scalar calibration and characterization of the Swarm magnetometry package. *Earth Planets and Space*, *68*(1), 129. https://doi.org/10.1186/s40623-016-0501-6